2011

Observations on braided thin wire nucleate boiling in microgravity

Justin P. Koeln
Utah State University

Jeffrey C. Boulware
Utah State University

Heng Ban
Utah State University

JR Dennison
Utah State University

Recommended Citation
Koeln, Justin P. and Jeffrey C. Boulware, Heng Ban and J.R. Dennison. Observations on braided thin wire nucleate boiling in microgravity. International Journal of Heat and Fluid Flow Volume 32, Issue 5, October 2011, Pages 973-981. 10.1016/j.ijheatfluidflow.2011.05.005

Observations on Braided Thin Wire Nucleate Boiling in Microgravity

Justin P. Koeln[a], Jeffrey C. Boulware[a], Heng Ban[a,*], J. R. Dennison[b]

[a]Department of Mechanical and Aerospace Engineering, Utah State University, 4130 Old Main Hill, Logan, UT 84322-4130, USA

[b]Physics Department, Utah State University, 4415 Old Main Hill, Logan, UT 84322-4415, USA

Abstract

A microgravity experiment was conducted on the Space Shuttle Endeavor (STS-108) to observe sustained nucleate boiling of water. Subcooled water was boiled with a single strand and a braid of three 0.16 mm diameter and 80 mm long Nichrome resistive wires. A CCD video camera recorded the experiment while six thermistors recorded the temperature of the fluid at various distances from the heating element. This paper reports experimental results in observations, measurements, and data analysis. Bubble explosions were found to take place shortly after the onset of boiling for both the single and braid of wires. The explosion may produce a high heat transfer rate, as it generates a cloud of micro-bubbles. The number, size, and departure rate of the bubbles from the heater wire were measured and compared with theoretical models as a function of time. The temperature measurements revealed a complex temperature distribution in the fluid chamber due to bubbles ejected from the wire that carried thermal energy close to the temperature sensors. Drag forces on departing bubbles were calculated based on bubble movement and used to predict bubble propagation. Results from this experiment provided further understanding of nucleate boiling dynamics in microgravity for the eventual design and implementation of two-phase heat transfer systems in space applications.

Keywords: microgravity; nucleate boiling; thin-wire; bubble departure; bubble explosion; drag forces.

Nomenclature

a	drag coefficient prediction constant
A	bubble cross-sectional area
A_c	contact area
C_d	coefficient of drag
D	bubble diameter
F_b	buoyant force
F_d	drag force
F_D	departure force
F_i	inertia force
F_m	Marangoni force
F_{net}	net force on bubble
F_p	pressure force
F_R	resistant force
F_s	surface tension force
g	gravitational acceleration
g_0	gravitational acceleration on Earth
K	Marangoni force coefficient
n	power in heat transfer coefficient model
R	bubble radius
R_0	wire radius
Re	Reynolds number
t	time
T'	temperature gradient
ΔT_{sub}	liquid subcooling
ΔT	temperature difference between heater wall and liquid
v	bubble velocity

Greek symbols

α	heat transfer coefficient
β	contact angle
μ_l	viscosity of water
σ	surface tension
σ_T	temperature coefficient of surface tension
ρ_l	density of liquid water
ρ_v	density of water vapor

Subscripts

b	buoyant
c	contact
d	drag
D	departure
i	inertia
l	liquid water
m	Marangoni
p	pressure
R	resistant
s	surface tension
sub	subcooling
T	temperature
v	water vapor
µg	microgravity
1g	Earth’s gravity

1. Introduction

Nucleate boiling is a well known, highly efficient mode of heat transfer used in many terrestrial heat transfer systems such as power generation, electronics cooling, and fluid handling and control. As technology advances toward the exploration and development of space, more robust, efficient, and cost effective heat transfer systems utilizing phase change are needed for space applications. The lack of free convection in space reduces convective heat transfer, thereby resulting in more localized heating and larger thermal gradients. Lack of buoyancy also increases the relative contributions of secondary forces such as surface tension, inertia, pressure, drag, and the Marangoni effect. These forces are heavily dependent on system characteristics such as the working fluid, level of subcooling, heat flux, and heating surface geometry; therefore, experimental results based on the characteristics of one system cannot be readily used to predict the results of another system. A fundamental understanding of the phase change characteristics is needed before heat transfer systems using nucleate boiling can be implemented in microgravity.

1.1. Review of microgravity boiling

As gravitation acceleration goes to zero, drastic reductions in heat transfer are predicted by the widely used empirical model for the efficiency of heat transfer for pool boiling (Eq. 1).

$$\frac{\alpha_{\mu g}}{\alpha_{1g}} = \frac{\Delta T_{1g}}{\Delta T_{\mu g}} = \left(\frac{g}{g_0} \right)^n \tag{1}$$

This equation shows that the heat transfer coefficient, α, for microgravity is proportional to the heat transfer coefficient on earth and the ratio of their respective gravitational accelerations raised to the n^{th} power. Using n = 0.5 and a microgravity value of $g = 10^{-4} g_0$, Rohsenow's relation predicts a heat transfer value of 1% of the terrestrial value [1].

Eq. 1 appeared to be verified by experiments performed by Tokura et al. [2], Fukada et al. [3], and Straub [5] where even at relatively low heat fluxes, large coalescing bubbles engulfed the heating elements causing the elements to dry out, overheat, and fail. In these experiments the bubbles acted like an insulating barrier, preventing heat from dissipating away from the heating element.

However, other microgravity experiments have proven that heat transfer is not reduced in microgravity and enhancements of up to 20% of the terrestrial value under the same conditions have been reported [6]. In these experiments, small bubbles form and grow on the heating element until they depart and transport heat away from the wire and into the surrounding fluid.

The dramatic difference in resulting heat transfer demonstrates the fact that boiling dynamics are heavily dependent on system characteristics such as working fluid, level of subcooling, heat flux, and heating surface geometry.

1.1.1. Fluid property and bubble dynamics

The forces that act on a bubble as it grows on the heating surface are heavily dependent on the properties of the working fluid. Zhao et al. [7] analyzed the forces on a bubble as it grows on a thin wire heating element under

normal and microgravity. The net force is dependent on the density of the liquid and vapor, surface tension, contact angle, and viscosity as shown in Eqs. (2) – (10).

$$F_{net} = F_D - F_R = (F_i + F_p + F_b) - (F_d + F_s + F_m) \tag{2}$$

The inertia force results from the growth of the bubble putting the surrounding fluid in motion. Eq. (3) shows the inertia force is equal to the mass of a sphere of liquid of the same radius as the bubble multiplied by the acceleration of the bubble radius (the leading negative sign corrects for the fact that the bubble radius growth is decelerating).

$$F_i = -\frac{4}{3}\pi R^3 \rho_l \frac{d^2R}{dt^2} \tag{3}$$

The pressure force, Eq. (4), results from the pressure difference between the inside the bubble and the surrounding fluid. The higher internal vapor pressure causes a force on the heating element creating a departure force.

$$F_p = \left(\frac{2\sigma}{R} + \frac{p_l R}{3}\frac{d^2R}{dt^2} + C_d \frac{p_l}{8}\left(\frac{dR}{dt}\right)^2 \right) A_c \tag{4}$$

The buoyancy force in Eq. (5), results from the difference between the density of the liquid and the vapor. Even though gravity levels of $10^{-3}g_0$-$10^{-5}g_0$ are quite small, the resulting buoyancy force could affect the total force on the bubble.

$$F_b = \frac{4}{3}\pi R^3 (\rho_l - \rho_v) g \tag{5}$$

The drag force is the resistance of the fluid on the wall of the bubble as the radius increases (Eq. 6).

$$F_d = C_d \frac{p_l}{2}\left(\frac{dR}{dt}\right)^2 A \tag{6}$$

The surface tension force, Eq. (7), is the force of adhesion between the water surrounding the bubble and the heating element

$$F_s = 4R_0 \sigma \sin^2 \beta \tag{7}$$

The Marangoni force, Eq. (8) is driven by the effects of temperature on surface tension. The surface tension of the warmer water near the heating element is less than surface tension of the cooler surrounding fluid. This creates a force acting to pull the bubble toward the heating surface.

$$F_m = 2K\pi \left|\sigma_T\right| T' R^2 \tag{8}$$

where the drag coefficient, C_d, and the contact area, A_c, in the equations above are calculated with Eq. (9) and (10), respectively.

$$C_d = 5{,}360\left(\frac{\rho_l R}{\mu_l}\frac{dR}{dt}\right)^{-0.79} \tag{9}$$

$$A_c = 4RR_0 \sin^2 \beta \tag{10}$$

Zhao's model appears to fit his data from a satellite experiment using subcooled R113. The physical properties of the fluid alter the bubble growth rate, departure diameter, and departure velocity during the boiling process. Under microgravity conditions, the effects of fluid properties on boiling dynamics have been demonstrated for various working fluids such as alcohols [8], water [3,8,9], R113 [7,10], and R134a [5].

1.1.2. Fluid subcooling

Fluid subcooling has been observed to affect bubble dynamics, heat transfer and the critical heat flux (CHF) in microgravity. The majority of microgravity experiments were performed at saturation temperature ($\Delta T_{sub} = 0$ K) in order to approximate steady state nucleate boiling; however, several experiments have analyzed the effects of subcooling with complementary results. Straub [6] reported the correlation between the subcooled and saturated heat transfer coefficients as a function of subcooling. The ratio of coefficients steadily increases with subcooling; reaching about 1.5 with a subcooling of about 30K. This relation appears to be the same for microgravity and terrestrial conditions.

Marangoni convection, thought to enhance heat transfer in the absence of natural, density-based convection, was observed by Straub [10] in subcooled boiling, but not in saturated boiling on a thin wire heater. Wan [11] observed the boiling of subcooled R113 and the presence of Marangoni convection. Wan reported that Marangoni effects led to bubble coalescence, often resulting in bubble departure thus distributing heat and preventing burn out. Each of these studies contributes to the notion that a heat transfer system with a subcooled working fluid would sustain a stable nucleate boiling, while saturated fluid would likely lead to burn out of the heater.

1.1.3. Heat flux

Sometimes, contrary to intuition, microgravity boiling has higher heat flux than normal gravity. Straub [10] has heavily researched the effects of heat flux on bubble behavior and heat transfer. Boiling subcooled R113 with a 0.2 mm diameter platinum wire, Straub's experiment compared the heat transfer coefficients in 1g and 0g using stepwise power capable of producing heat fluxes of 17, 39, and 77 kW/m^2. In 0g, nucleate boiling occurred very quickly at 17 kW/m^2; however, in 1g, free convection was sufficient to cool the wire and boiling did not occur until 77 kW/m^2. At 77 kW/m^2, a 6% enhancement of the heat transfer coefficient was observed in 0g.

In another experiment by Straub [5], boiling R134a with 0.05 and 0.2 mm diameter platinum wire, heat transfer increased 10% in the 0g experiment when compared to the 1g experiment, for the 0.2 mm wire in at 50 kW/m^2, which steadily decreased as heat flux was increased to 350 kW/m^2. The 0.05 mm wire had a fairly constant reduction in heat transfer of approximately 10% and burn out occurred at 250 kW/m^2.

Fukada et al. [3] also observed wire burn out. Using a 0.2 mm diameter platinum wire to boil saturated water, burn out occurred at a heat flux of 120 kW/m^2. The burn out was caused by a large coalescing bubble that engulfed the heating element minimizing heat transfer.

1.1.4. Heater surface geometry

Surface modification, providing bubble nucleation enhancement, increases heat transfer under microgravity boiling, which is similar to cases under normal gravity. Several experiments have evaluated the effects of various surface geometries on heat transfer and boiling dynamics. Fukada et al. [3] observed the difference in bare platinum

wires and wires with calcium carbonate scale and its effects on heat transfer and CHF. During boiling with the bare wires, coalescing bubbles formed that engulfed the wire, resulting in burn out. On the scaled wire, small individual bubbles were observed, which detached from the wire and burn out was prevented. The scaled wire was able to perform at heat fluxes exceeding the CHF of the bare wire; therefore, CHF was effectively increased due to the scale. These results were attributed to the higher wettability and nucleation site density of the scale wire.

In summary, there have been quite a number of studies on boiling in space and the conclusions are not all consistent. Understanding underpinning mechanisms is the key to the rationalization of inconsistent and sometimes conflicting observations. In order to better understand boiling in microgravity, more experiments on different conditions are needed with more qualitative and quantitative information. This study provides further observations of boiling using a unique heating surface.

1.2. Objectives

This Space Shuttle experiment was performed with the following objectives:

1. Observe the nucleate boiling from single and braided thin heating wires in sustained microgravity,

2. Obtain size, position, velocity, and acceleration data from visual recordings of the nucleate boiling process in microgravity, and

3. Verify drag force equations to analytically predict the propagation of bubbles after departing the wire.

2. Experimental apparatus

The sustained microgravity environment during the Space Shuttle mission, enabled close measurement of a highly stable system. Shown in Fig. 1, the experiment consisted of a polycarbonate fluid chamber with a rear Viton rubber expansion wall. The two heating elements span the chamber vertically and are made of Nichrome C (61% Ni, 15% Cr, bal. Fe) with a diameter of 0.16 mm and a length of 80 mm. The braided heating element consisted of three of these wires.

Six YSI 441107 Teflon-encapsulated thermistors were positioned at various distances from the heating elements, shown in Fig. 2, and recorded temperature once every minute. A CCD camera visually recorded the boiling and was digitized at 15 frames per second and 720 x 540 pixel resolution, with a pixel size of 0.1 mm x 0.1 mm.

Initially, the fluid chamber was held at 14.7 psi (1 atm) and the water was heavily subcooled with a ΔT_{sub} = 78.8 K. The water was deionized but the presence of dissolved gases is unknown. The braided heating element was powered by 5.5 volts, generating a heat flux of 160 kW/m^2 and the single wire was powered by 12 volts, generating a heat flux of 775 kW/m^2. The braided wire was powered for 35 min, followed by 1 hour of cool down, and then the single wire was powered for 35 min. For these power levels and duration, the fluid pressure is assumed to be held constant and any volumetric thermal expansion was accommodated by the rear Viton rubber expansion wall. The residual gravity level on the Space Shuttle is negligible, reported to be $10^{-3}g_0$-$10^{-5}g_0$ [7,12], which generated an even distribution of bubbles in the fluid chamber.

3. Results, analysis, and discussion

3.1. Bubble explosion

Several bubble explosions (Fig. 3) were observed within the first few minutes of boiling for both the braided wire and single wire experiments. These explosions varied in size and consisted of a bubble rapidly expanding, often stretching along the direction of the wire, and then breaking into many very small bubbles (0.1 – 0.2 mm diameter). The entire sequence lasted approximately 0.13 sec. (2 video frames) and it is believed that the bubble explosion phenomenon occurred where coalesced bubbles generated on the heated surface at high heat flux were broken into many microbubbles. Such violent explosions of bubbles have not been reported in the literature on microgravity boiling. The 'cloud' of microbubbles after the explosion, as shown in Fig. 3, is similar to what happens for microbubble emission boiling when the surrounding liquid has a high degree of subcooling [13]. Because of the sustained microgravity, a heavy degree of subcooling (ΔT_{sub} = 78.8 K) was able to exist in this experiment. This rarely studied level of subcooling allowed a very large thermal gradient to remain in the fluid chamber for a prolonged period of time.

By simulating the temperature gradients in the fluid chamber using ANSYS, a finite element analysis software, large changes in fluid temperature were predicted across the diameter of the bubble. Figure 4 shows the result of the conduction calculation of water using 6.47 kW/m^2 heat flux at 2 min after the start of heating. In the experiment, the several bubbles that exploded were approximately 2.0 mm in diameter prior to explosion, which were a subset of all the bubbles in the chamber at this time. The model used a much lower heat flux than the actual experiment since phase change was not simulated. At this point in the experiment, a pure conduction model can be used because of the spares formation of bubbles along the wire. Conduction is still the primary heat transfer method at 2 min. Even with this much lower heat flux there could exist as much as a 50 K temperature difference across the diameter of the bubbles. This temperature gradient could cause instability in the vapor-liquid interface and could be one of the mechanisms causing the bubble surface to collapse, resulting in the observed explosion.

Bubble explosions could greatly enhance the heat transfer. Many ground experiments have studied the phenomena similar to bubble explosion, which is often referred to as bubble collapse or microbubble emission boiling (MEB). The phenomena were first observed in 1986 by Inada et al. [14] and further research has shown that MEB can remove up to 14.41 MW/m^2 at a mass flux (of phase change) of 883.8 kg/m^{2}s, proving to be a promising method for the cooling of microelectronic chips [13]. Shoji and Yoshihara [15] discovered that MEB occurs with subcooling greater than 40K on Earth. Although MEB is different from the bubble explosion observed in this study, it does provide potential insight into the conditions for the bubble to explode and potential benefit of increased heat transfer rate. Even though the absence of convection in space creates larger thermal gradients, previous pool boiling experiments probably did not have the required degree of subcooling to observe such phenomenon.

However, the physical understanding and mathematical description of the bubble explosion phenomenon still need to be developed. Further experiments in microgravity must be performed to develop a better understanding of bubble explosions so the phenomenon can be used in the development of highly efficient heat transfer systems.

3.2. Bubble population

After 2 min of power to the braided wire, 18 bubbles of at least a 0.1 mm diameter were observed in the visible section of the fluid chamber (shaded area of Fig. 2) with an average measured diameter of 0.8 mm. A significant

increase in the number of visible bubbles was observed between 2 and 4 min; however, the average bubble diameter remained fairly constant. From 4 to 10 min, the number of bubbles remained fairly constant, but the average diameter steadily increased to 1.6 mm. After 10 min of power, overpopulation of bubbles made tracking the number and size of bubbles difficult.

Bubble departure rate was also observed to vary with time. Within the first few minutes of power, only small individual bubbles departed the wire at sparse intervals. Between 5 and 20 min, coalescence between adjacent bubbles was noticed and rarely caused the departure of the coalesced bubble. After 20 min, thousands of small (0.1-0.2 mm) bubbles departed the wire along with several very large bubbles (4-6 mm). These large bubbles existed only in the absence of buoyancy. Experiments performed by Qui et al. [10] showed that departure diameters up to 20 mm are possible in microgravity. Most of the bubbles left the wires radially, but several departed at sharp angles due to the influence of adjacent bubbles. Most remained less than 25 mm away from the wire, but several propagated to the walls of the chamber (38 mm) over time.

This experiment indicated that the ejection of bubbles from the heater wire was sustained in microgravity. There was no formation of a single large bubble engulfing the heater wire and causing it to burn out as observed in some of the microgravity boiling experiments. A high degree of subcooling in this experiment could be one of the reasons for the result. In addition, the bubbles departed without a preferred direction. An even spread of bubbles existed throughout the fluid chamber, indicating that the residual gravity had little effect on the growth or propagation of the bubbles during this experiment.

Without gravity, the majority of growth of bubbles in the experiment appeared to be heat transfer controlled, instead of inertia controlled. Although the initial formation and growth of the bubble may be inertia controlled, most of the bubble growth appears to be governed by heat transfer, as indicated by bubble growth proportional to $t^{1/2}$, as shown in Fig. 5. Excluding the first measured data point and given that the accuracy of bubble diameter measurement is ±0.1 mm, the heat transfer controlled bubble growth curve fits all of the measured data points. If bubble growth was inertia controlled, an increase in heat would not result in an increase in bubble growth, which could result in the burn out of the heating element.

The total bubble volume with respect to time was also determined. Figure 6 shows the correlation of the measured total volume of vapor in the visible area with respect to time for the first 10 min of boiling. The R^2 value of 0.9974 reveals that constant heat flux produces a constant volume of vapor. As long as the wall effects did not interfere, this linear relation indicated that quasi-steady state nucleate boiling had been achieved.

3.3. Temperature profiles

Each of the 6 thermistors shown in Fig. 2 measured the temperature of the water once per minute throughout the experiment. Figure 7 shows the temperature readings for 4 thermistors (L1, L3, R1, R3); data from L2 and R2 were excluded because these thermistors experienced hardware failures. The recorded temperatures did not change when bubbles first appeared on the braided wire during the first 9 min. In this time interval, the water adjacent to the wire was slightly above saturation temperature while these four points, the closest being 6.4 mm from the wire, were still at about 21°C. Due to the lack of major convective flow, conduction was likely the main mechanism for heat

transfer. When more bubbles began ejecting from the wire, a convective flow of bubbles and water resulted, causing thermistor temperatures to start to rise after ~15 min. Because of the inhomogeneous and erratic nature of bubble ejection and transport, the sensor temperature responses were somewhat irregular. If a bubble travelled in the vicinity of a given sensor, the temperature of that sensor rose faster as a result. After 35 min, the power was turned off and temperatures decreased due to cooling. However, because the thermistors had relatively large thermal mass, and because they were influenced by the bubbles travelling to them, sometimes attaching to them, the temperature readings show a general trend with high level of irregular fluctuations.

The power for the single wire was about three times that of the braided wire causing the temperature to increase almost immediately. The recorded water temperature never surpassed 70°C, thus remaining 30°C below saturation temperature due to the absence of buoyancy-driven convective flow.

3.4. Thermal model predictions

Because the braided wire had a unique configuration, the center region was likely heated to a higher temperature and generated early phase change. The finite element analysis software, ANSYS, was used to model the braided wire system. The model was used to look at the heating dynamics around the three wires and was limited to conductive heat transfer of the water and the wire and did not include the effects of phase change. The purpose of this model was to observe the temperature distribution around the three wire geometry during the initial liquid heating phase, before phase change was present, to see if the center region reached saturation temperature more quickly than other locations on the heating element. The modeling domain was a circle with the radius of 40 mm, 250 times the wire diameter. This radius was chosen because the temperature at 40 mm does not change over the 35 min run time. There were 27,166 grids consisting of unstructured grids between the wires and structured grids in the wires and around the wires. A 0.05 s time step was used and the solution was expected to be independent of time and grid spacing. The results were checked to ensure that they are independent of grid size and time step.

Figure 8 shows the relative temperature distribution surrounding the three braided wires based on the ANSYS simulations. The interior region surrounded by the wires reaches saturation temperature within 1 s after power is provided. The area near the touching point between two wires also reaches saturation temperature very quickly and is likely where the first bubbles nucleate. This quick achievement of saturation temperatures in the interior of the three wires leads to the rapid generation of bubbles. The braided wires could initiate bubbles without the need for large superheating of whole surfaces due to the concentration of heat flux in the center of the braid. Therefore, further research may prove a braid of wires to be an effective form of bubble generation, which is an innovative approach in this experiment.

3.5. Bubble propagation

Bubble propagation data were obtained from pictures extracted from the video. Five bubbles which appeared to travel on the plane perpendicular to the camera were analyzed. The sizes of the bubbles upon departure were 1.5 mm, 1.5 mm, 2 mm, 1.6 mm and 1.4 mm for Bubbles 1, 2, 3, 4, and 5, respectively, with ±10% uncertainty due to camera resolution and lighting conditions. Figure 9 shows an example of a picture created from the video file with

Bubble 3 in the upper right comer. Position data for each bubble were taken from the visual recording of the experiment and velocity and acceleration data were obtained using a first-order, center differencing approach. Upon departure from the heating surface, the bubble decelerates due to the drag force (Eq. 11) exerted by the quiescent water.

$$F_d = -\frac{1}{2}\rho_l v^2 A C_d \tag{11}$$

Classic bubble dynamics estimates the bubble mass as 11/16 of the mass of the fluid that would occupy the space of the bubble. This estimation, developed by Han and Griffith [16], accounts for fluid carried with the bubbles during transit in microgravity. Thus, assuming negligible phase change at the bubble's surface after leaving the wire, the force balance becomes,

$$-\frac{1}{2}\rho_l v^2\left(\frac{\pi}{4}D^2\right)C_d = \frac{11}{16}\rho_l\left(\frac{1}{6}\pi D^3\right)\frac{dv}{dt} \tag{12}$$

as shown in Eq. (12). Simplified, the equation becomes,

$$\frac{dv}{dt}v^{-2} = -\frac{12}{11}\frac{C_d}{D} \tag{13}$$

Several models exist which attempt to numerically predict the drag coefficient for a bubble at various Reynolds numbers. Gorring and Katz [17] presented a number of correlations based on the function

$$C_d = \frac{a}{\mathrm{Re}} \tag{14}$$

where the constant *a* is dependent on the flow regime. Moore's relation assumes a = 32 and was used for this study within its limited range of Reynolds numbers. A more recent model by Kelbaliyev and Ceylan [18] integrates the full regime of $0.5 < \mathrm{Re} < 100$ as shown below:

$$C_d = \frac{16}{\mathrm{Re}}\left[1+\left(\frac{\mathrm{Re}}{1.385}\right)^{12}\right]^{1/55} \tag{15}$$

Figure 10 shows the difference between these two models and the standard model for a solid sphere. The Kelbalilyev model was consistently smaller at all Reynolds numbers, while the Moore's model is in between.

Secondary forces, such as the Marangoni force, were neglected for the modeling of bubble propagation. Throughout the bubble's trajectory the drag force is an order of magnitude greater than the Marangoni force due to low thermal gradients once the bubble leaves the vicinity of the wire.

The predicted paths of a bubble after departing the heater wire determined using Moore's relation and the Kelbaliyev model are presented in Fig. 11. It is evident that both models generally agree with the experimental data, although Moore's model tends to yield more travelling distance than the Kelbaliyev model. This is due to the fact that the initial Reynolds number of the departing bubbles is greater than 30, a critical point in Fig. 10 where the Moore and Kelbaliyev curves intersect. When the bubbles first depart, the high Reynolds number results in Moore's model predicting a lower drag coefficient than the Kelbaliyev model. Since the bubbles trajectory is highly

dependent on the drag force during the high initial velocities, Moore's model will always predict more travel since the initial drag coefficients are lower. Both prediction curves tend to plateau slightly quicker than the measured data for all five bubbles. For the empirically determined model inputs, Moore's relation initially overestimated the bubble position for approximately the first second after leaving the wire. Conversely, the Kelbaliyev model always under predicted the displacement of the bubble for all five bubbles. The prediction paths for bubbles with a lower initial velocity appeared to fit the measured data most accurately.

3.6 Bubble Condensation

Due to the high degree of subcooling, it is expected that these bubble would condense much more rapidly than observed. Based on the degree of subcooling the vapor bubbles should have condensed within several seconds after departure from the wire. Clearly this was not the case, as bubbles from the braided wire experiments were present during the single wire experiment after the one hour cooling period. Dissolved air contamination would be the only cause for this resistance to condensation. Unfortunately, the composition of dissolved air is an unknown variable in this experiment. The propagation models above are valid for bubbles that maintain a constant diameter as observed in the video recordings of this experiment.

3.7. Discussion

The absence of buoyancy allows nucleate boiling dynamics to be controlled by secondary forces. These secondary forces are heavily dependent on experimental characteristics; therefore, results from one experiment may not extrapolate to another scenario without a fundamental understanding. This study verified several conclusions from previous experiments which can be used to create a general understanding of the nucleate boiling phenomenon independent of system characteristics.

One of the unique features of this experiment is the heavy degree of subcooling. Previous experiments [6] have shown that higher degrees of subcooling can reduce the tendency to form a large coalescing bubble engulfing the heater, which often results in heater burn out. Subcooled fluid experiments produce small individual departing bubbles, while saturated fluid experiments produce large coalescing bubbles. The current experiment appeared to verify this conclusion in that the steady ejection of bubbles was observed. Small individual bubbles formed and departed throughout the duration of the experiment and heater burn out was prevented. Several of the departure and resistant forces in Eqs. (2) - (8) are dependent on properties such as surface tension and density which vary with temperature and based on these results, subcooling appears to be a driving force behind bubble departure for microgravity boiling. Therefore, it is important to include the effect of subcooling in the force analysis of bubble departure.

Large bubble departure diameters are associated with microgravity experiments [10] and are present in the current experiment. Without the departure force of buoyancy, the resistant forces can hold a bubble on the wire longer, generating larger diameters. It is expected that, under certain conditions, these resistant forces will be greater than the departure forces for any bubble diameter, and the bubble will continue to grow on the heating surface until a dry out and failure occur. In this experiment, the departure forces were larger than the resistant forces; therefore, dry out and failure did not occur.

Previous microgravity experiments also conclude that CHF is drastically reduced in microgravity. Experiments by Kim et al. [4] and Straub [5,10] have shown significant decreases in CHF up to 50% of the terrestrial value. CHF has also been shown to increase with experimental factors such as subcooling [4] and surface geometry enhancements such as scale [3]. The CHF of the current experiment was not reached due to the heavy subcooling and vigorous departure of small bubbles throughout the experiment.

Some aspects of microgravity nucleate boiling are highly case dependent and conclusions from previous experiments have been contradictory. For example, many experiments such as ones performed by Straub [5,10] and Wan and Zhao [19] concluded that bubble departure is mainly due to the inertia caused by bubble coalescence. Other experiments [7,12] concluded that bubble departure can be predicted by the net force on the bubble (Eq. 2). The current experiment has observed both types of departure. Bubble coalescence was observed to cause bubble departure, however many bubbles appear to depart on their own once they reach a certain size. Further experimental and modeling study is needed to develop a theory for bubble departure.

Finally, as previously stated, microgravity boiling heat transfer is controlled by secondary forces, which are a function of the system's working fluid, subcooling, heat flux, and surface geometry. Therefore, it is acceptable that different experiments would produce different effects on heat transfer due to differences in these parameters. Several experiments have shown that heat transfer can be enhanced by increasing the surface area of the heating element by using scale or micro-pin-fins. These surfaces produce small areas of superheated fluid where phase change is initiated; therefore, the surface as a whole can remain at a relatively low superheat and bubble generation and growth can still occur. Wire superheat was not measured in the current experiment and therefore heat transfer enhancement could not be concluded. However, the braided wire geometry is expected to increase heat transfer because of its unique feature of localized superheated center area. This internal area of superheating is likely to enhance bubble generation and growth without increasing surface superheat of the external area.

4. Conclusions

Based on the results and analyses of the STS-108 experiment on nucleate boiling, several of which are first to be reported, the following overarching conclusions can be made:

1. Bubble explosion and microbubble emission is possible in microgravity, occurring at a heat flux of 163 kW/m^2 for the braided wire and 775 kW/m^2 for the single wire with heavily subcooled conditions. This paper includes the first report of pool boiling bubble explosions in microgravity.

2. Bubble radius growth is measured to be proportional to $t^{1/2}$, indicating the heat transfer controlled regime of bubble growth, and total vapor volume is linear with respect to time under constant heat flux.

3. A bubble can be ejected from a heated wire in the absence of gravity, due to the departure force overcoming the resistant forces at various bubble sizes.

4. The unique configuration of a braided wire heating element enhances bubble generation and conduction-induced thermal gradients within the water; this may lead to a fundamentally new approach to bubble generation and heat transfer enhancement.

5. The temperature distribution without buoyancy is affected by bubble insulation on the heating wire, as well as bubble movement and heat transport caused by bubble propagation, resulting in a complex temperature field.

6. Models based on Moore's relation and the Kelbaliyev equation for bubble drag can both accurately describe travel from a thin wire in zero gravity, within the limited spatial resolution of this study.

While this study adds significantly to the understanding of nucleate boiling of water in sustained microgravity, clearly further research is needed to develop better understandings of the nucleate boiling process under various fluid, surface, and heat flux conditions under microgravity.

Reference

[1] W.M. Rohsenow, A method of correlating heat transfer data for surface boiling of liquids, Transactions ASME, Series C, Journal of Heat Transfer 74 (1952) 969.

[2] I. Tokura, Y. Hanaoka, H. Suzuki, H. Hirata, M. Yoneta, Boiling heat transfer on thin wires in a microgravity field, Proceedings of the ASME/JSME Thermal Engineering Conference, Maui, HI, 1995, pp. 555-560.

[3] Y. Fukada, I. Haze, M. Osakabe, The effect of fouling on nucleate pool boiling of small wires, Heat Transfer-Asian Research 33 (5) (2004) 316-329.

[5] J. Straub, Bubble – bubbles - boiling, Microgravity Science and Technology 16 (1) (2005) 242-248.

[6] J. Straub, Boiling heat transfer and bubble dynamics in microgravity, Adv. Heat Transfer 35 (2001) 57-172.

[7] J.F. Zhao, G. Liu, S.X. Wan, N. Yan, Bubble dynamics in nucleate pool boiling on thin wires in microgravity, Microgravity Science and Technology 20 (2008) 81-89.

[8] H. Wang, X. Peng, S.V. Garimella, D.M. Christopher, Microbubble return phenomena during subcooled boiling on small wires, International Journal of Heat and Mass Transfer 50 (2007) 163-172.

[9] J.F. Lu, X.F. Peng, Bubble separation and collision on thin wires during subcooled boiling, International Journal of Heat and Mass Transfer 48 (2005) 4726-4737.

[10] J. Straub, Highs and lows of 30 years research of fluid physics in microgravity, a personal memory, Microgravity Science and Technology 18 (3) (2006) 14-20.

[11] S. Wan, J. Zhao, G. Liu, Dynamics of discrete bubble in nucleate pool boiling on thin wires in microgravity, J. Thermal Sci. 18 (1) (2009) 13-19.

[12] J.F. Zhao, S.X. Wan, G. Liu, N.Yan, W.R. Hu, Subcooled pool boiling on thin wire in microgravity, Acta Astronautica 64 (2009) 188-194.

[13] G. Wang, P. Cheng, Subcooled flow boiling and microbubble emission boiling phenomena in a partially heated microchannel, International Journal of Heat and Mass Transfer 52 (2009) 79-91.

[14] S. Inada, Y. Miyasaka, S. Sakamoto, G.R. Chandratilleke, Liquid-solid contact state in subcooled pool transition boiling system, Journal of Heat Transfer 108 (1986) 219-221.

[15] M. Shoji, M. Yoshihara, Burnout heat flux of water on a thin wire, Proceedings of the 28th National Heat Transfer Symposium of Japan, 1991, pp. 121-123.

[16] C. Han, P. Griffith, The mechanism of heat transfer in nucleate pool boiling, International Journal of Heat and Mass Transfer 8 (1965) 887-904.
[17] R.L. Gorring, D.L. Katz, Bubble rise in a packed bed saturated with liquids, American Institute of Chemical Engineers Journal, 8 (1) (1962) 123-126.
[18] G. Kelbaliyev, K. Ceylan, Estimation of the minimum stable drop sizes, break-up frequencies, and size distributions in turbulent dispersions, Journal of Dispersion Science and Technology 26 (2005) 487-494.
[19] S.X. Wan, J.F. Zhao, Pool boiling in microgravity: recent results and perspectives for the project DEPA-SJ10, Microgravity Science and Technology 20 (2008) 219-224.

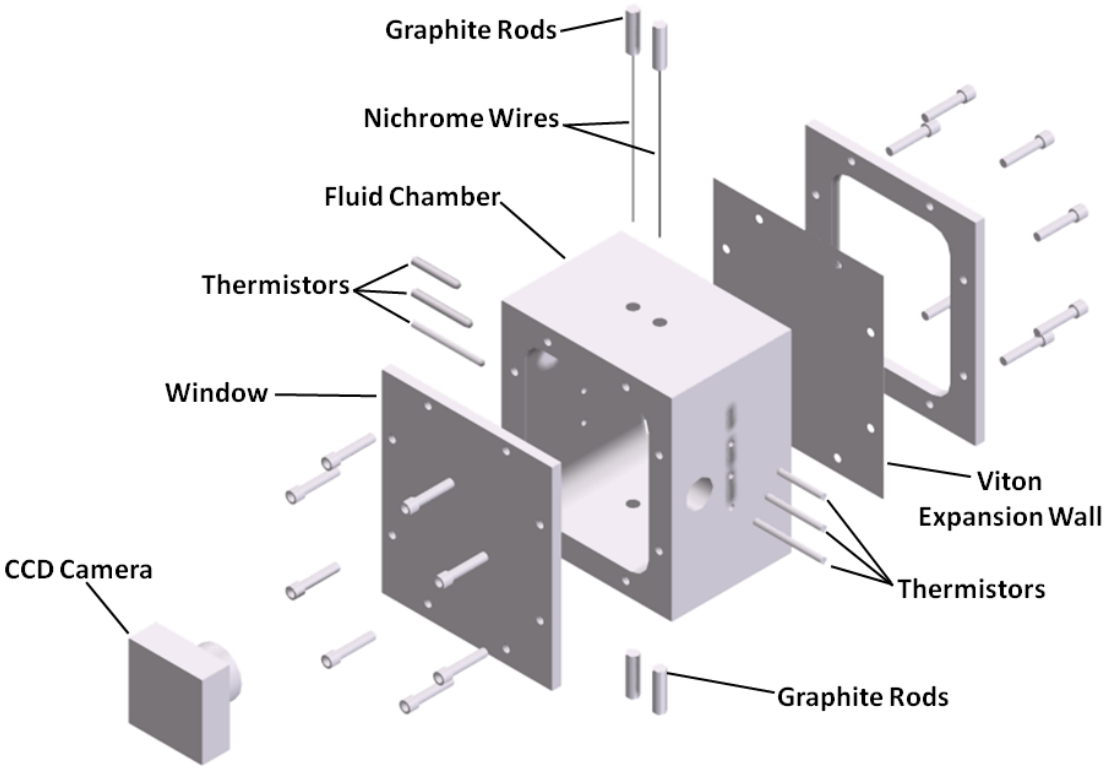

Fig. 1. Diagram of experimental fluid chamber.

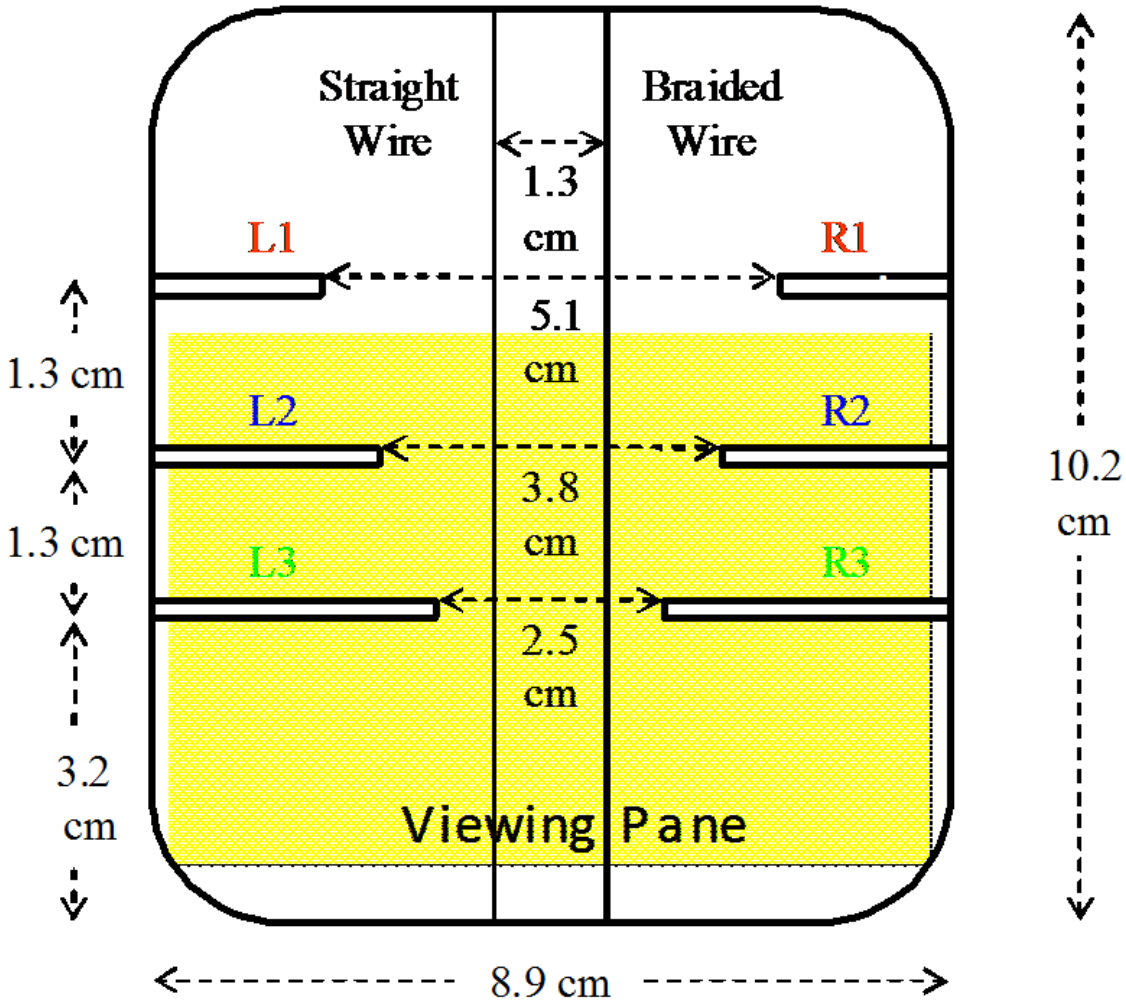

Fig. 2. Chamber cross section schematic.

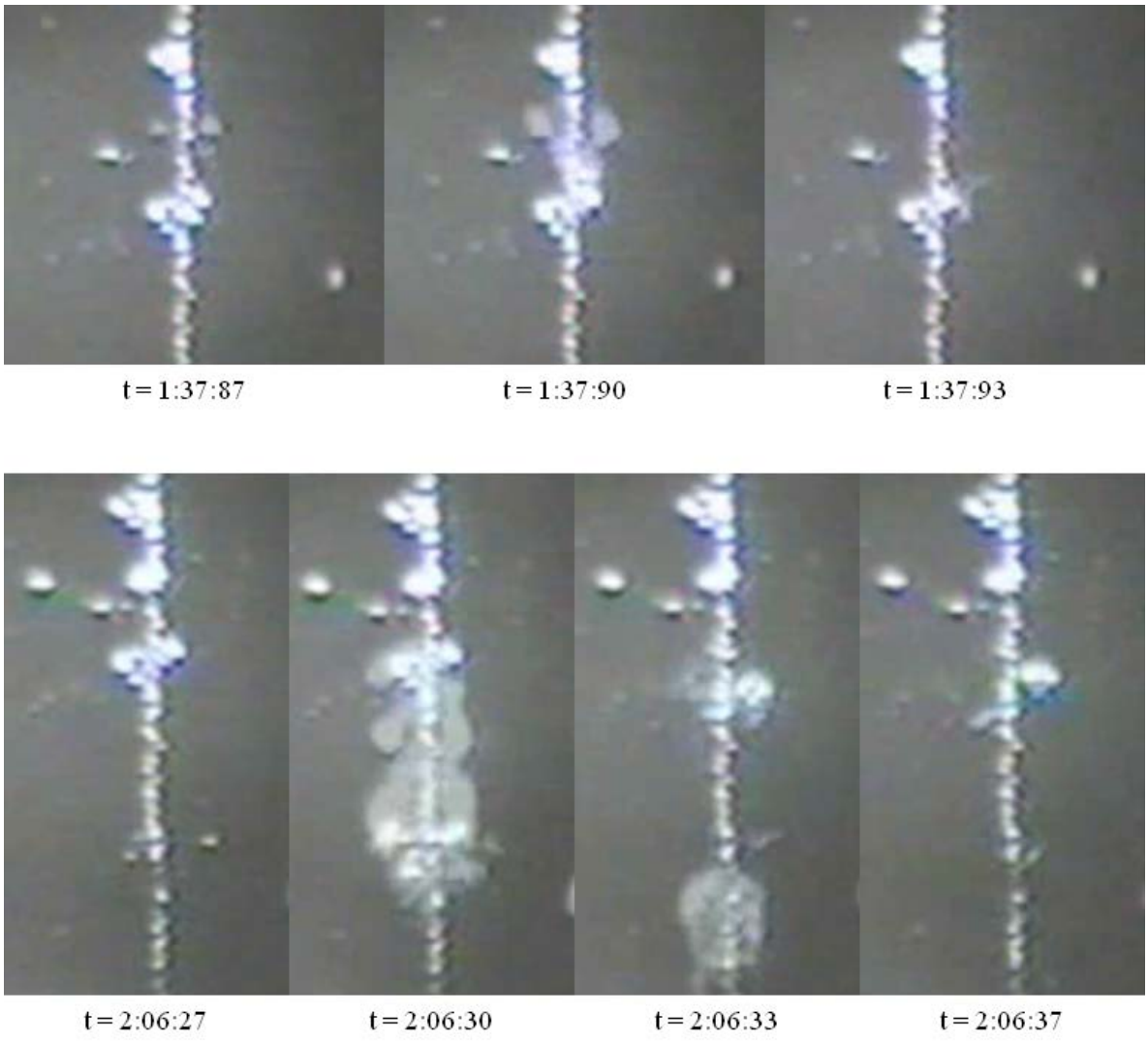

Fig. 3. Photographs of two bubble explosions.

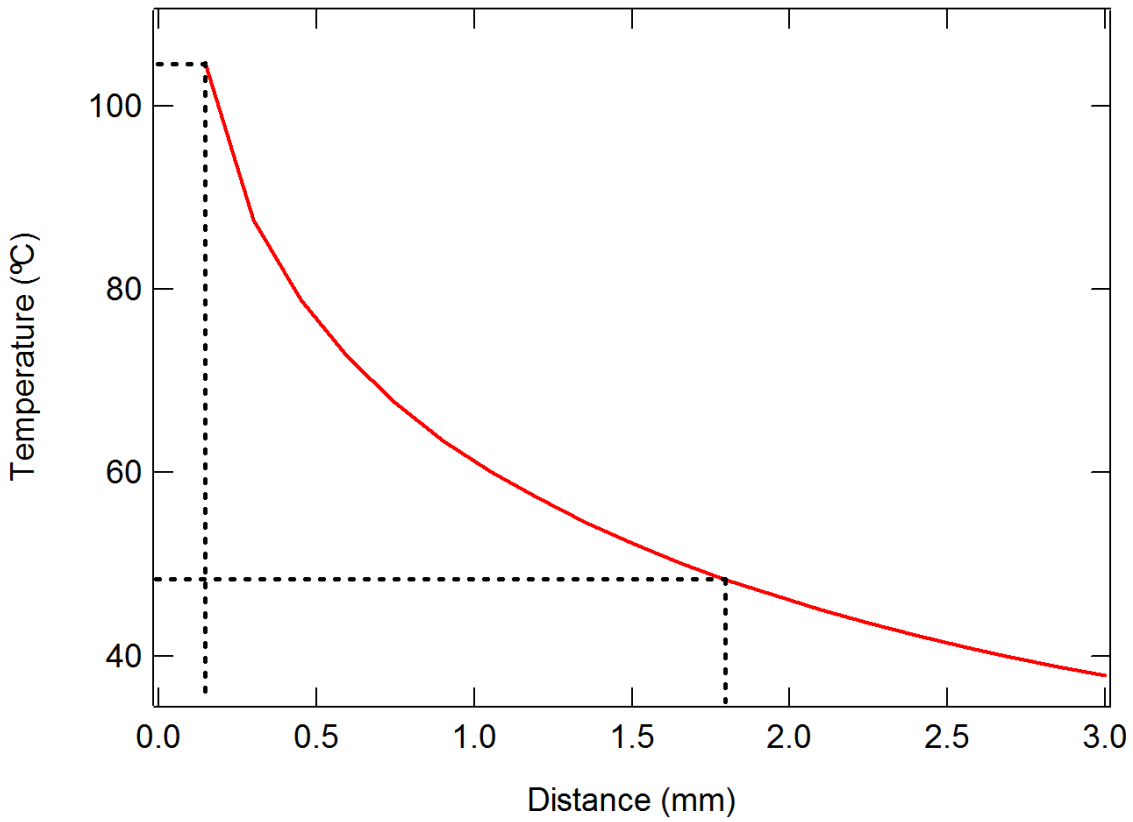

Fig. 4. Temperature of fluid versus distance from center of braided wires from ANSYS modeling.

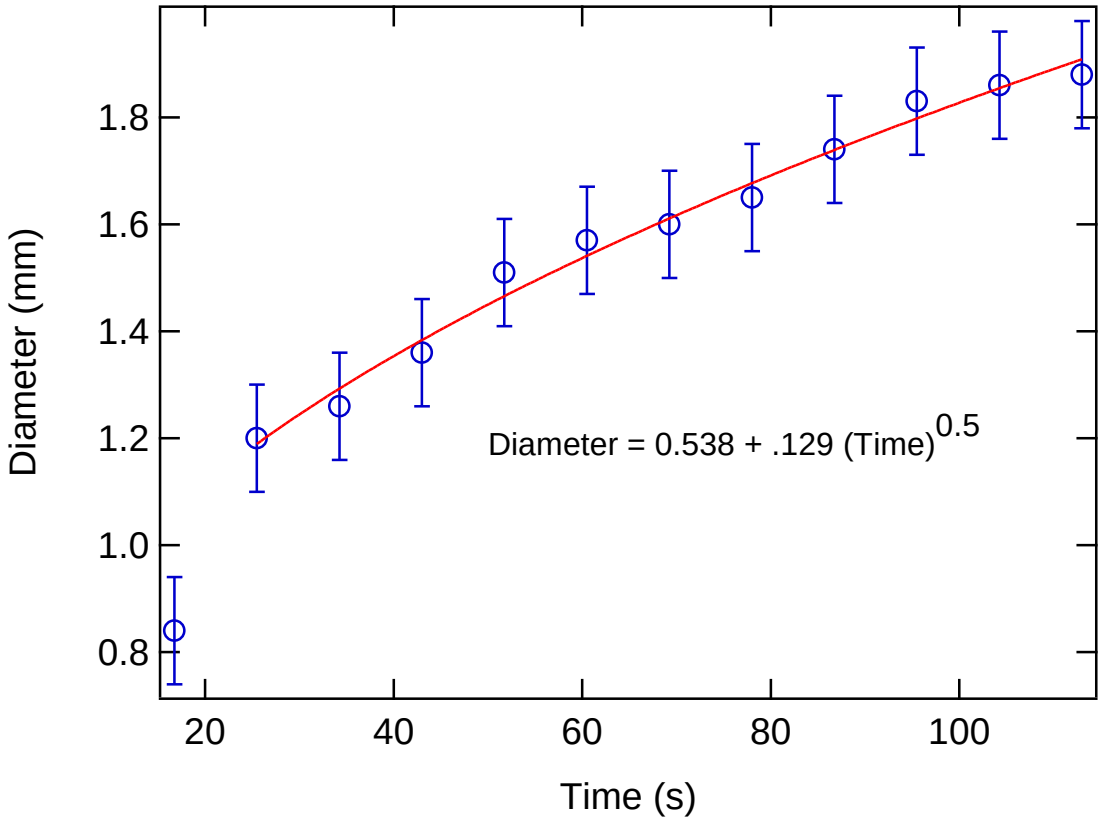

Fig. 5. Measured bubble diameter with respect to time compared to predicted bubble growth.

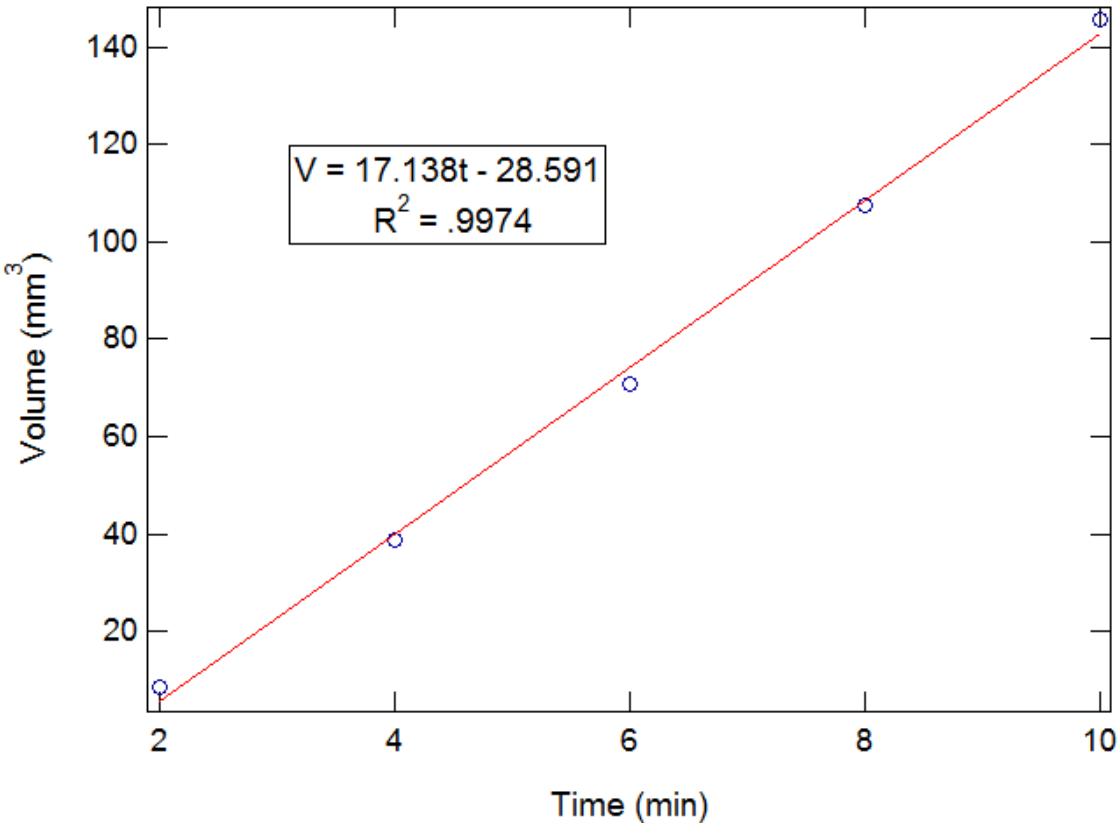

Fig. 6. Total volume of vapor in fluid chamber versus time.

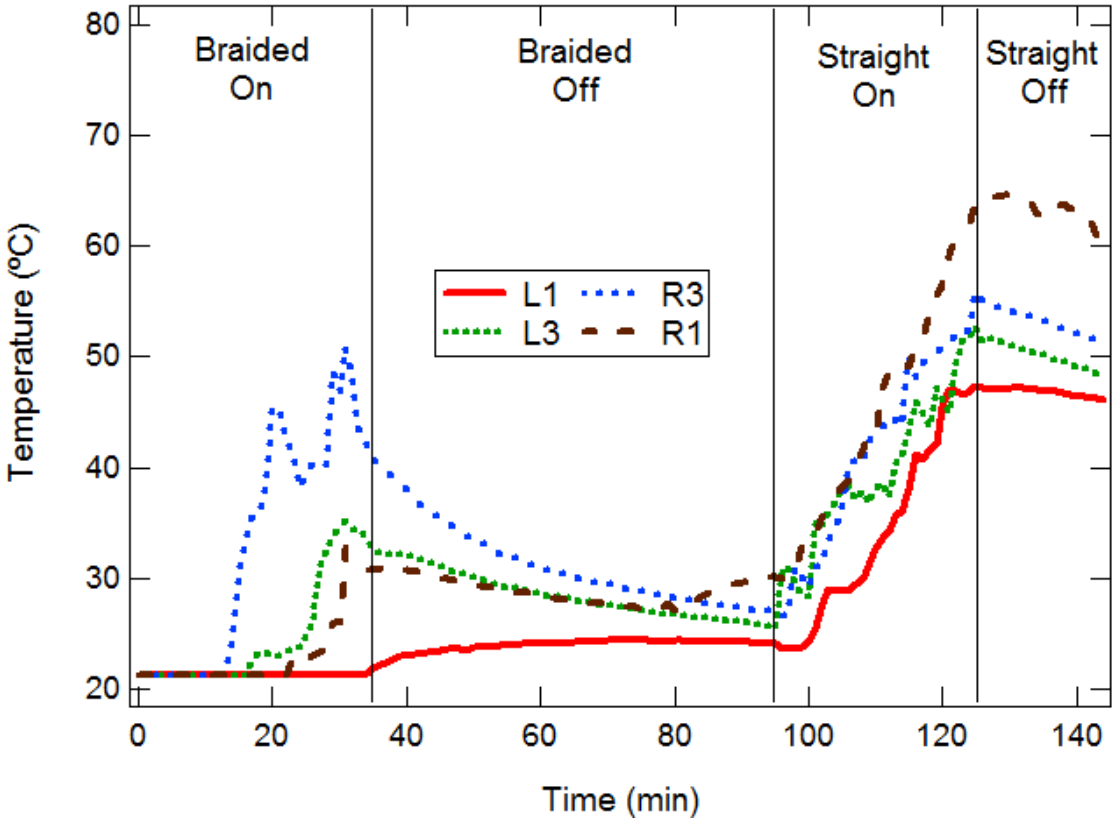

Fig. 7. Thermistor readings over time (refer to Fig 2. for thermistor locations).

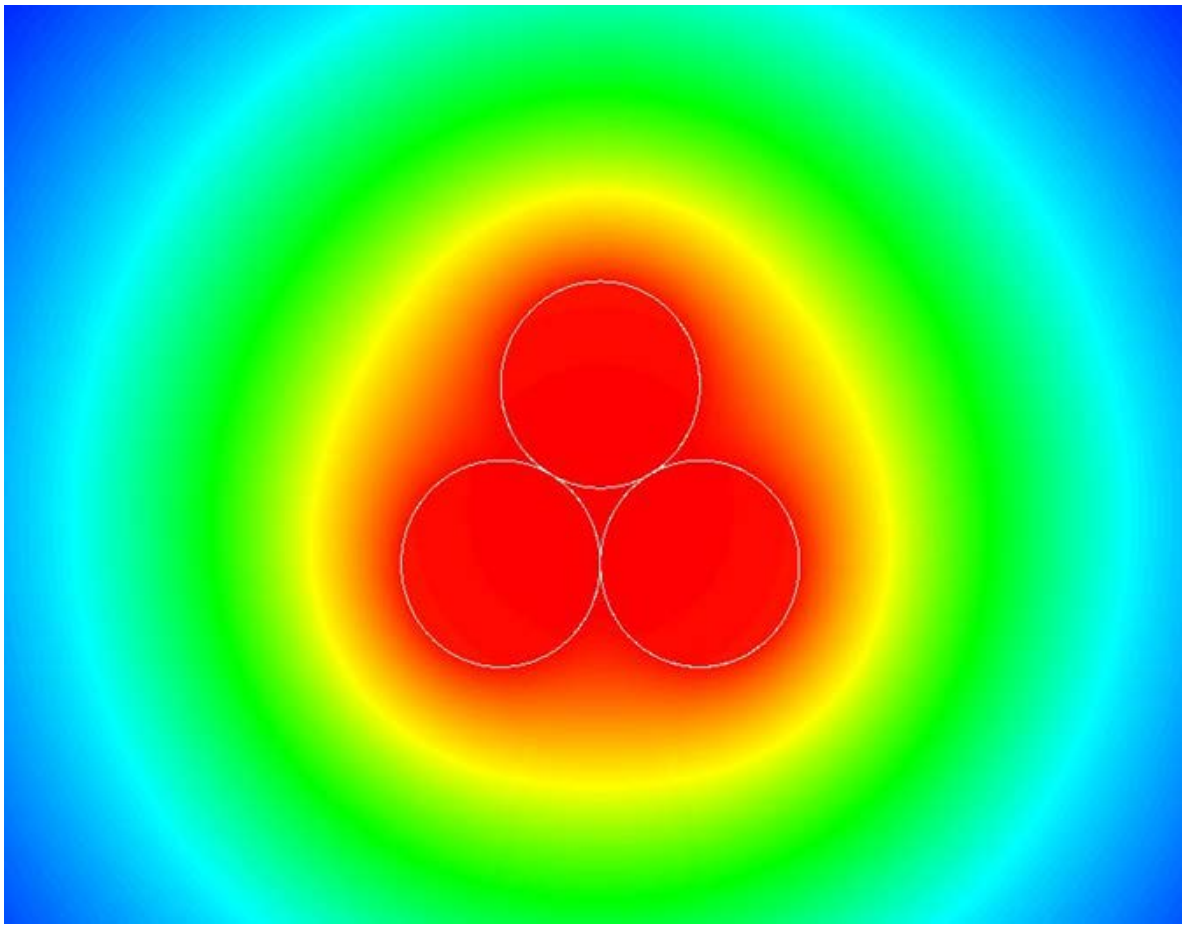

Fig. 8. Temperature contours surrounding the 3 heating wires (D = 0.16 mm) at time t = 120 s.

Fig. 9. Photograph of nucleate boiling on a braided wire.

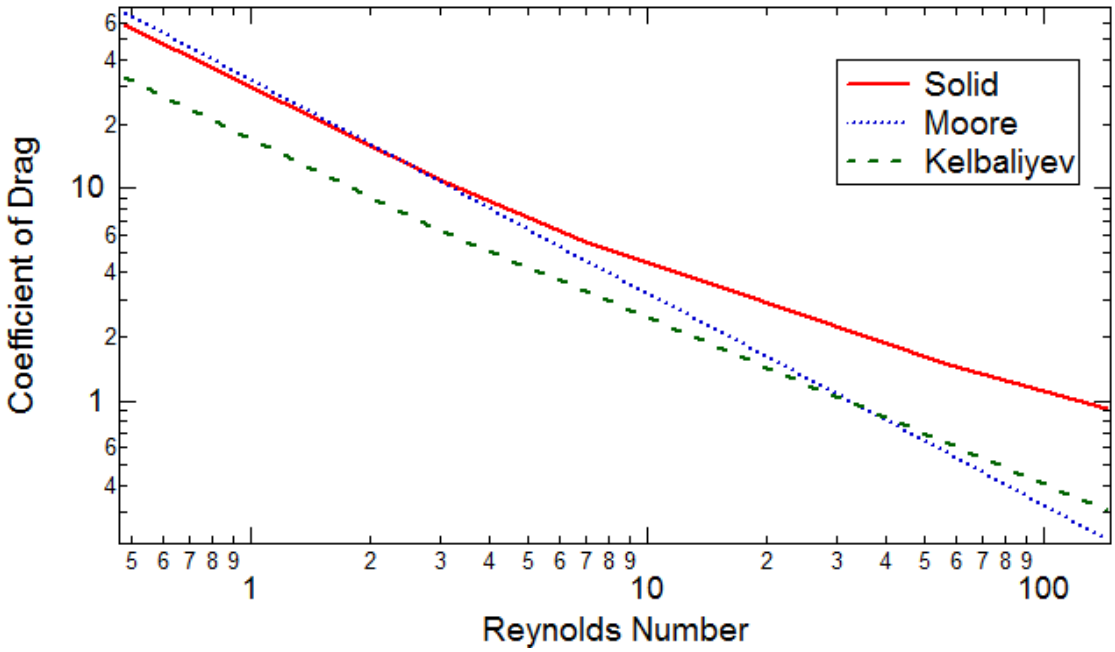

Fig. 10. Comparison of drag coefficient for a solid sphere and a bubble using Moore's and Kelbaliyev's methods.

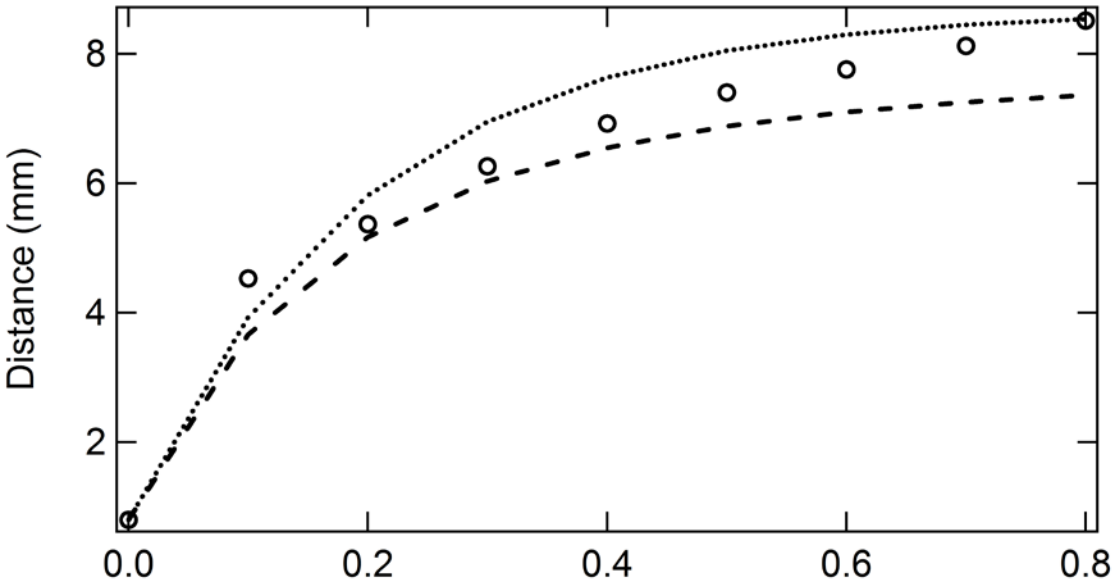

(a)

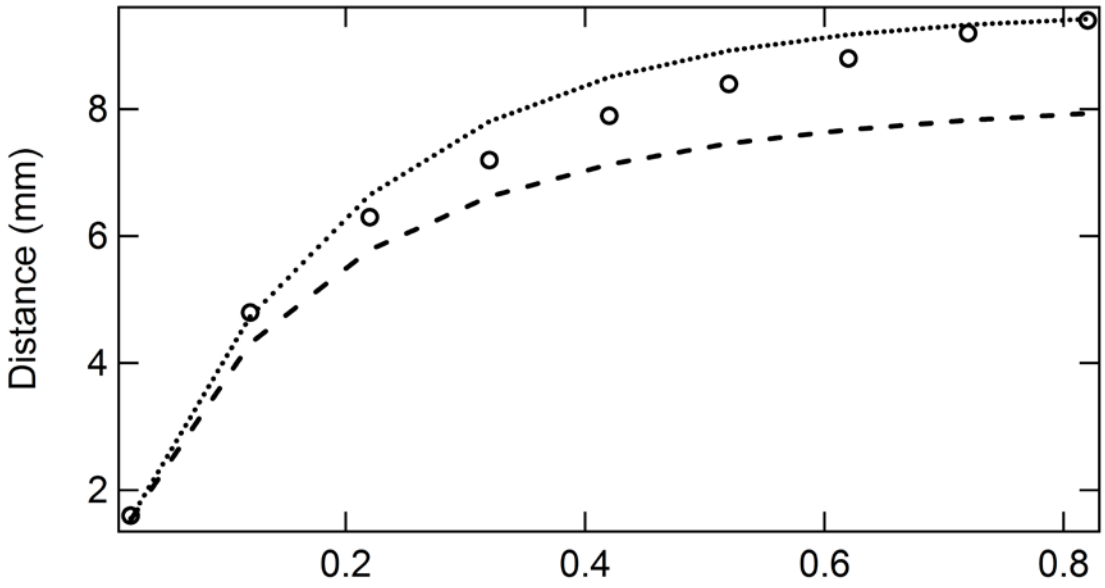

(b)

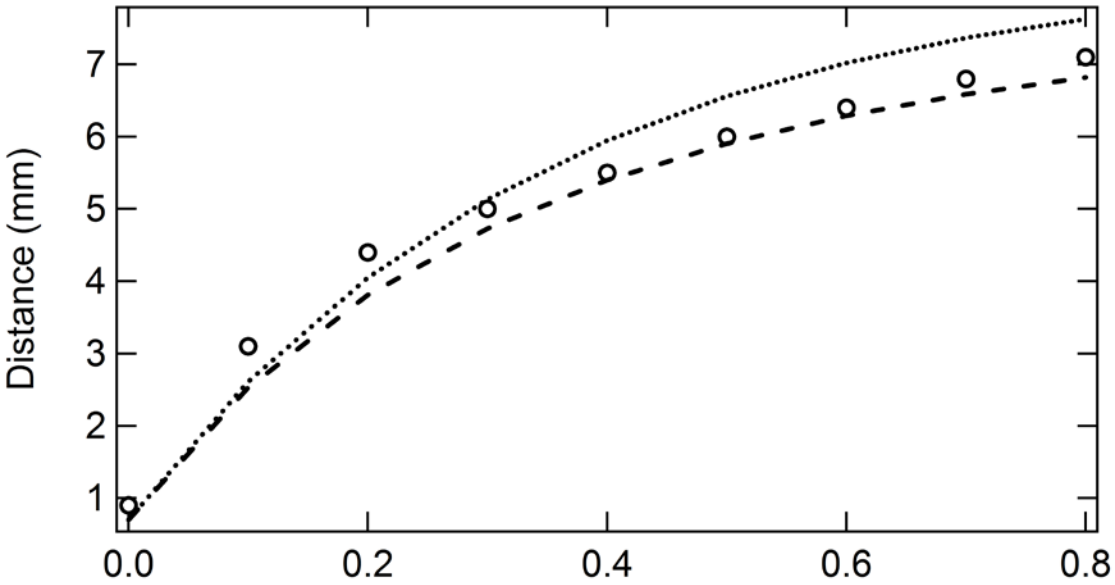
Distance (mm)
1
2
3
4
5
6
7
0.0
0.2
0.4
0.6
0.8

(c)

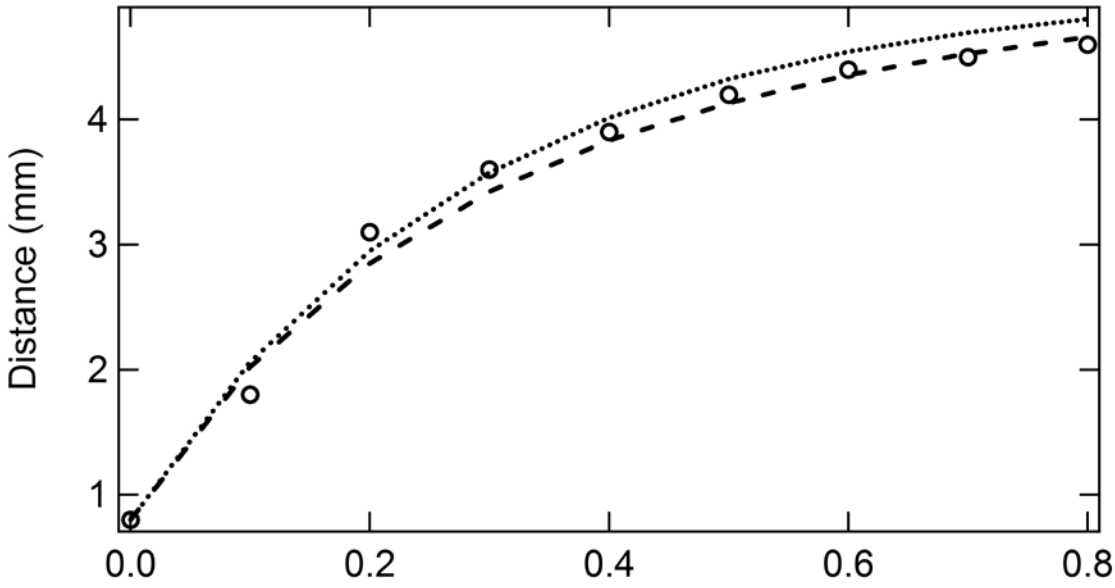
Distance (mm)
1
2
3
4
0.0
0.2
0.4
0.6
0.8

(d)

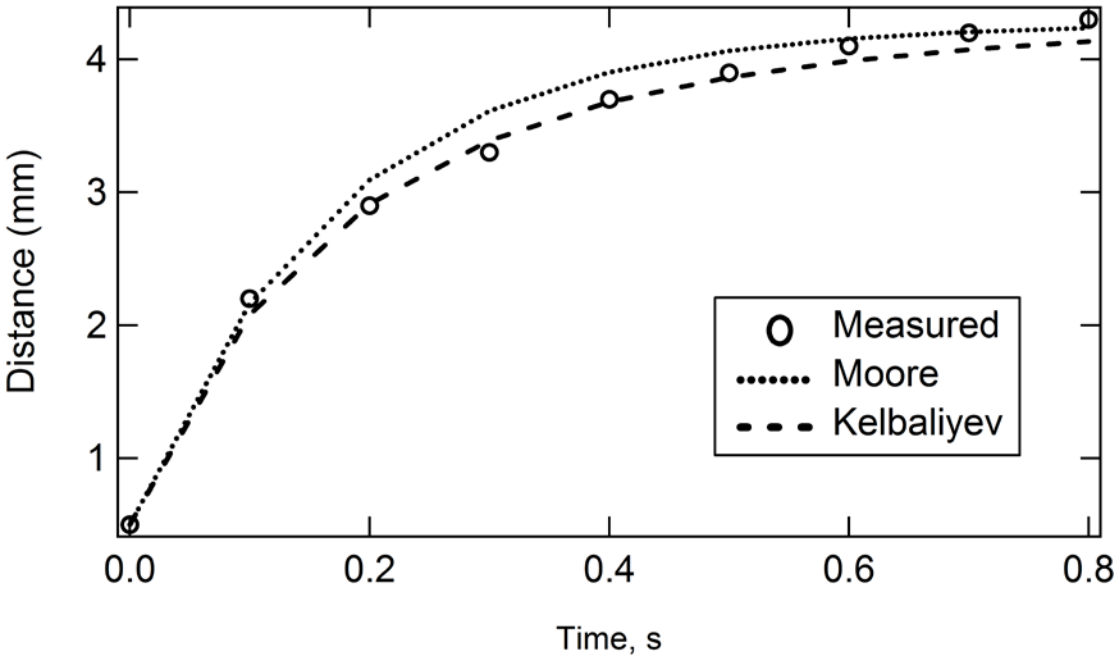

(e)

Fig. 11. Measured and predicted displacement over time. (a) Bubble 1, D = 1.5mm (b) Bubble 2, D = 1.5mm (c) Bubble 3, D = 2.0 mm (d) Bubble 4, D = 1.8mm (e) Bubble 5, D = 1.4mm.